ISSN: 2319-6505

Available Online at http://journalijcar.org

International Journal of Current Advanced Research
Vol 5, Issue 12, pp 1554-1559, December 2016

RESEARCH ARTICLE

International Journal of Current Advanced Research

ISSN: 2319 - 6475

SPECTROSCOPIC PROPERTIES OF $_x$MgO- 10Nb_2O_5-(89-x)TeO_2-1CuO GLASS SYSTEM

Chinna Babu J[1]* and Vedavyas S[2]

[1]Physics Research Laboratory, Department of Physics, Government City College, Osmania University, Hyderabad-500 002, Telangana state, INDIA
[2]Department of Physics, Osmania University, Hyderabad-500 002, Telangana state, INDIA

A R T I C L E I N F O

Article History:

Received 18th September, 2016
Received in revised form 5thOctober, 2016
Accepted 16th November, 2016
Published online 28th December, 2016

A B S T R A C T

The preparation and structural studies were undertaken on the xMgO- 10Nb_2O_5-(89-x)TeO_2-1CuO glass system containing Cu^{2+} as spin probe. Differential scanning calorimetry (DSC), Infrared (IR), Electron Spin Resonance (ESR), Raman and optical absorption studies have been carried out. Glass transition temperature (T_g) of glass samples have been estimated from the DSC measurements and it has been found that T_g increasing with the MgO content. From IR and Raman spectra, it is clear that, present glass system consists of structural units of TeO_3 (tp) and TeO_4 (tbp) and NbO_6 octahedra. TeO_4 units are found to be converted into TeO_3 units with increasing MgO content. From ESR spectra it is clear that the Cu^{2+} ion is in tetragonal distorted octahedral site with $d_{x^2-y^2}$ as ground state. Bonding parameters and bonding symmetry have been calculated from both optical absorption and ESR data and are found to change with increase in MgO content.

INTRODUCTION

A tremendously intense research is going on Tellurium oxide based glasses due their peculiar properties like high refractive index, low phonon energy, high dielectric constant, good infrared transmission and large third order non-linear susceptibility. They have been considered as the best materials for use in memories, laser hosts and non-linear optical devices like optical amplifiers and optical filters [1-3].

Glasses containing Nb_2O_5 also have technological importance for many device applications due to their interesting optical and electric properties [4-5]. Alkali niobium tellurite glasses and glass ceramics have shown extremely interesting non-linear optical properties and these glasses are suitable for making optical waveguide devices.

The structure of tellurite glasses is of interest because their basic structural unit is an asymmetrical TeO_4 trigonal bipyramid with a lone pair of electrons in an equatorial position, and the content of network modifier changes the coordination number of the tellurium ion with respect to oxygen ions. This change leads to a TeO_3 trigonal pyramid, which is considered to restrict the glass formation [6].

Optical properties of glasses based on TeO_2 and heavy metal oxides have stirred up significant interest in the field of new glassy materials and have become promising materials for some optoelectronic applications. Tellurium oxide glasses with metal oxide like MgO and PbO shows several interesting characteristics. They are potential materials for up-conversion lasers, optical fiber amplifiers and nonlinear optical devices. Duverger et al. studied the effect of the doping metal on the structure of binary tellurium oxide glasses with MgO, PbO and ZnO [7]. Komatsu et al. studied the temperature dependence of refractive index and electronic polarizability of RO- TeO_2 glasses (R = Mg, Ba, Zn) [8].

In the present study, xMgO-10Nb_2O_5-(89-x)TeO_2-1CuO glasses where x = 5 to 25 mol% have been prepared and characterized by using spectroscopic techniques like infrared, Raman, ESR and optical absorption.

Experimental

Glasses with the composition of xMgO- 10Nb_2O_5-(89-x) TeO_2-1CuO where x = 5 to 25 mol%, were prepared and characterized. The detailed compositions of the glasses under study are presented in table 1.

Table 1 Composition of *xMgO- 10Nb_2O_5-(89-x)TeO_2-1CuO glass* system

Glass label	Composition
MNT1	5MgO-10Nb_2O_5-84TeO_2-1CuO
MNT2	10MgO-10Nb_2O_5-79TeO_2-1CuO
MNT3	15MgO-10Nb_2O_5-74TeO_2-1CuO
MNT4	20MgO-10Nb_2O_5-69TeO_2-1CuO
MNT5	25MgO-10Nb_2O_5-64TeO_2-1CuO

Appropriate amounts of analar grade MgO, Nb_2O_5 and TeO_2 were taken into a mortar and ground thoroughly for homogeneous mixing. 1 mol% CuO was added as a spin probe and melted in a platinum crucible at 800-950 ^oC for 40 min in an electrical furnace. Melts were stirred frequently for high homogeneity and were poured onto a steel plate maintained at 250 ^oC and pressed quickly with another steel plate to a thickness of about 1mm. Glass samples were transferred to annealing furnace and are annealed at 250 ^oC for 4 hours to avoid mechanical strains and cracking, in the sample.

X-ray diffraction patterns for all the glass samples were recorded using copper target (K_α = 1.54A°) on Philips Panaltic X' Pert at room temperature.

Density of all the samples is measured at RT using the Archimedes method with xylene as an immersing medium. The measured densities are reproducible to ±0.01g/cm^3. The molar volume is calculated from the relation $V_m = \frac{M}{\rho}$, where M is the molar mass of glass and ρ is density of the glass.
From the density data, oxygen packing density is calculated using the following formula.

Oxygen packing density = $\Sigma x_i n_i / V_m$, where x_i is the molar fraction of an oxide R_mO_n and n_i number of oxygen atoms of this oxide. The glass transition temperature T_g was measured using a temperature differential scanning calorimeter (TA Instruments DSC 2010). All samples were heated at the standard rate of 10 °C min^{-1} in aluminum pans.

Infrared transmittance of all powder glass samples (glass and KBr mixed pellets) were recorded by using Perkin-Elmer FT-IS spectrometer model 1605, in the wavenumber range of 400-4000 cm^{-1} at RT.

The RT Raman measurements were performed in the range of 100-1600 cm^{-1} on micro Raman system using Jobin-Yvon Horiba (LABRAM HR-visible) spectrometer. Ar^+ laser beam of 488 nm (E = 2.53 eV) was used for the excitation. The incident laser power is focused in a diameter of 1-2µm and a notch filter is used to suppress Rayleigh scattered light.

ESR spectra of powdered glass samples were recorded on X-band at room temperature by using JEOL-JES FE 3X ESR spectrometer, with 100 KHz field modulation. DPPH was used as a standard g marker.

Optical absorption spectra of all glasses were recorded on Shimazdu UV-3100 spectrometer in the wavelength range of 200-1000 nm at RT using air as a reference medium. The 'Peak-pick' facility provided in the spectrometer was used to measure the peak positions.

RESULTS AND DISCUSSION

XRD spectra

Fig. 1 shows the XRD pattern of the present glass system. No sharp peaks have been observed in the X-ray diffraction patterns of the glass samples; however they contain two broad curves, typical of structures without long range order. Hence, it is confirmed that present glass systems are amorphous in nature.

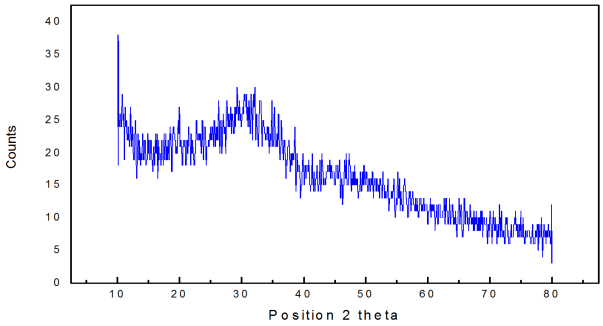

Fig.1 Typical XRD spectra of MNT glass series

Density, molar volume and oxygen packing density

Physical parameters like average molecular weight, molar volume and oxygen packing densities are evaluated for all glass samples and are tabulated in Table 2 and from this table it is clear that all physical parameter values are increasing with MgO content. Fig.2 shows the variation of density with MgO content of the glass series. Densities are increasing linearly with substitution of MgO. Molar volume linearly decreases with increase in MgO content. Oxygen packing densities of all glass samples are increasing with MgO content.

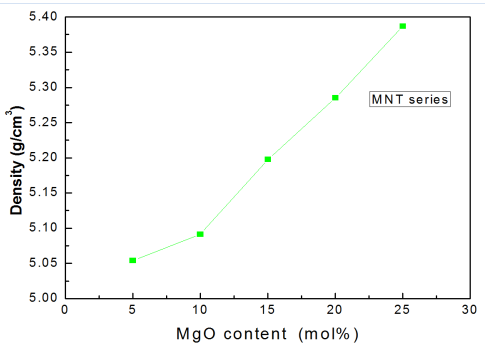

Fig.2 Variation of density with MgO content of MNT glass series

Table 2 Average molecular weights, densities (ρ), molar volumes (Vm), Oxygen packing densities (OPD), glass transition temperatures (Tg), Onsetcrystallization temperatures (Tx) and glass stabilities for the xMgO-10Nb2O5-(89-x)TeO2-1CuO glass system .

Glass label	Avarage molecular weight (g/mol)	Density (ρ) (gm/cm^3)	Molar volume (V_m) (cm^3/mol)	OPD($\bar{O}$) (g-at/l)	Glass transition temp. (T_g) (°C)	Onset cryst. temp. (T_x) (°C)	Glass stability (ΔT) (°C)
MNT1	163.455	5.05	32.340	69.26	375	479	104
MNT2	157.490	5.09	30.932	70.40	389	485	96
MNT3	151.525	5.19	29.15	73.40	415	497	82
MNT4	145.56	5.28	27.541	75.58	419	453	34
MNT5	139.595	5.38	25.912	78.72	425	447	22

Differential scanning calorimetry

DSC thermograms of the glass system xMgO-10Nb_2O_5-(89-x)TeO_2-1CuO are shown in Fig.3.

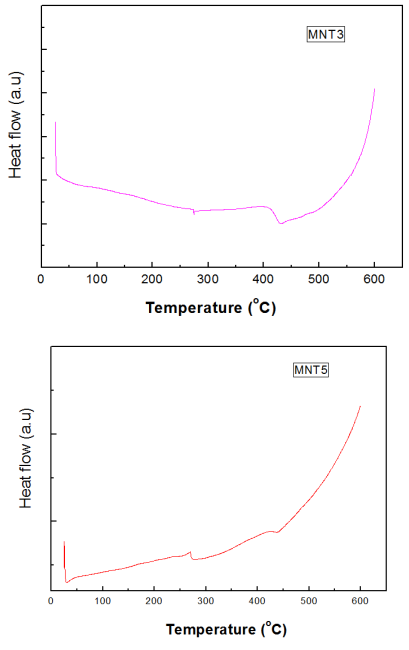

Fig.3 DSC plots of MNT1 glass series.

The DSC curves for the glasses show a very broad endothermic hump corresponding to the glass transition temperature, T_g, starting of crystallization is called onset crystallization temperature, T_x and other endothermic event corresponding to the melting temperature T_m. The T_g data of the glasses are given in Table 3.

The glass transition temperature increases from 375 to 425°C for present glass system with increase in the MgO content. The reason for increase in the T_g is that Nb-O-Te and Nb-O-Nb linkages are increasing, requiring higher temperature for relaxation. Furthermore, oxygen packing density also increases with MgO content. The tightness of packing in the oxide network decides the glass transition temperature. Thus with increase of MgO content, tightness of the glass increase leads to the increase in glass transition temperature. The difference between the onset of crystallization temperature (T_x) and glass transition temperature is $\Delta T = (T_x - T_g)$, has frequently been quoted as a rough indicator of glass stability. It represents the temperature interval during which nucleation takes place. From table 2 it is clear that glass stability decreases as the MgO content increases in the present glass systems.

Infrared spectra

The infrared spectra of the glass system is shown in figure 4. The significant bands are observed at 624-641, 677-696, 752-779, 892-914 and 1002-1020 cm^{-1}. The peak positions of the glasses are presented in table 3 and the band assignments of glass series is given in table 4.

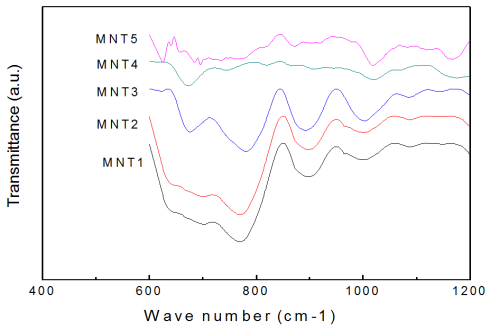

Fig 4 Infrared spectra of *xMgO- 10Nb$_2$O$_5$-(89-x)TeO$_2$-1CuO glass* system.

Table 3 Peak positions from infrared spectra for *xMgO-10Nb$_2$O$_5$-(89-x) TeO$_2$-1CuO glass system*

Glass label	Peak positions (cm^{-1})				
MNT1	641	696	771	892	1002
MNT2	641	694	772	899	1002
MNT3	-	673	779	892	1003
MNT4	-	677	752	909	1020
MNT5	622	682	772	914	1020

Table 4 IR band assignments of MNT glass series

Region of IR bands (cm^{-1})	Assignments
624-641	TeO_4 trigonal bipyramids
677-696	TeO_3 trigonal pyramids
752-779	Presence of NbO_6 octahedra
892-914	Vibration of Nb in NbO_6 octahedra

The structure of TeO_2 - rich glasses consists of TeO_4 trigonal bipyramidal building units, where one equatorial site is occupied by a pair of electrons and the equatorial oxygen in one unit is the axial site of the next, in analogy with α-TeO_2. In the present glass system, the absorption band at 624-641 cm^{-1} can be assigned to the Te-O_{ax} bond in TeO_4 trigonal bipyramid and this band shifts towards 677-696 cm^{-1}, which is characteristic peak of Te-O bond in TeO_3 trigonal pyramids, as MgO content increases. This clearly indicates that TeO_4 trigonal bipyramid units are converting to TeO_3 trigonal pyramids with increase in MgO content. Thus the introduction of MgO destroys the three-dimensional network by creating non-bridging oxygen (NBO) species and gradually transforming the TeO_4 units into TeO_{3+1} and TeO_3 [9,10]. The band at 752-779 cm^{-1} is due to the presence of NbO_6 octahedra. The band around 892-914 cm^{-1} is assigned to the vibration of Nb in NbO_6 octahedra and its neighboring non-bridging oxygen [11, 12].

Raman spectra

The Raman spectra of glass system xMgO-10Nb$_2$O$_5$-(89-x)TeO$_2$-1CuO are shown in figure 5, in the wave number range of 100-1200 cm^{-1}. The peak positions of Raman spectra of the glass system are presented in table 5 and the band assignments of the glass system is given in table 6.

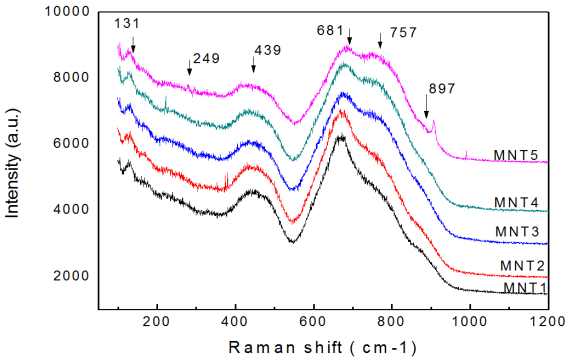

Fig. 5 The Raman spectra of *xMgO- 10Nb$_2$O$_5$-(89-x)TeO$_2$-1CuO glass* system

Table 5 Peak positions of Raman spectra for *xMgO-10Nb$_2$O$_5$-(89-x)TeO$_2$-1CuO glass* system

Glass label	Peak positions (cm^{-1})					
MNT1	128	249	445	674	773	871
MNT2	125	236	449	674	763	874
MNT3	128	236	439	674	760	864
MNT4	125	229	436	678	760	881
MNT5	131	249	439	681	757	897

Table 6 Raman band assignments for MNT glass series.

Region of Raman bands (cm^{-1})	Assignments
229-246	Vibrations of Nb-O-Nb in NbO_6 octahedra
436-449	Symmetric vibrations of Te_{eq}-O_{ax}-Te_{eq}
674-681	TeO_4 trigonal bipyramids
757-773	TeO_3 trigonal pyramids
864-897	Bending modes of Nb-O-Nb in NbO_6 octahedra

In Raman spectra, six major Raman absorption bands are observed at around 125-131, 229-246, 436-449, 674-681, 757-773 cm^{-1} and 864-897 cm^{-1}. The bands around 229-246 cm^{-1} is attributed to the vibration of Nb-O-Nb in NbO_6 octahedra. The bands around 436-449 cm^{-1} is assigned to the symmetric stretching vibrations of Te_{eq}-O_{ax}-Te linkage. Intensity of this band gradually increases with increase in MgO content, which can be assigned to increase in the Te-O-Te and Te-O-Nb bridging bonds, which would increase the

network connectivity in agreement with the T_g increase [13, 14].

The bands observed at 674-681cm^{-1} are due to the stretching band of tellurium and axial oxygen (Te-O_{ax}) in TeO_4 trigonal bipyramids (tbp) and bands at around 757-773 cm^{-1} are assigned to Te-O stretching mode in TeO_3 trigonal pyramids (tp) [15]. At low concentrations of MgO, the glass structure mainly consists of TeO_4 trigonal bipyramids making up a continuous network. When the MgO content increases, the band intensity at 674-681cm^{-1} decreases while intensity at 757-773 cm^{-1} increases. This change clearly indicates that the tellurium network is converting from TeO_4 (tbp) units to TeO_3 (tp) units via an intermediate coordination called TeO_{3+1} where, one Te-O_{ax} distance is elongated while the opposite is shortened. This conversion of TeO_4 (tbp) units to TeO_3 (tp) units is also evidenced from IR spectra.

A band resolved at around 864-897 cm^{-1}in all glass samples is due to the bending modes of Nb-O-Nb bonds found in the octahedral structure of NbO_6 and symmetrical stretching vibrations of Nb-O bonds found in NbO_6 octahedra [16].

ESR spectra

The Electron Spin Resonance (ESR) is a very powerful technique for investigating paramagnetic centers in oxide glasses containing transitional metal oxides and is useful for identifying the local environment of a paramagnetic impurity and mapping the crystal-field. The ESR spectra for the glass series is shown in figure 6.

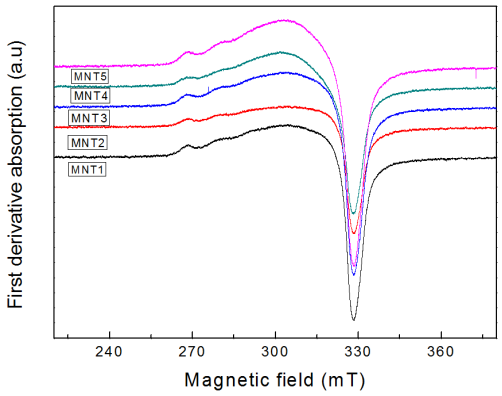

Fig. 6 The ESR spectra of Cu^{2+} in *xMgO- 10Nb_2O_5-(89-x)TeO_2-1CuO glass* system.

The spectra closely resembles that of Cu^{2+} in most oxide glasses, which can be easily recognized on the basis of four line hyperfine splitting due to ^{63}Cu and ^{65}Cu (I = 3/2), but isotope splitting is not resolved owing to nearly identical nuclear moments. The hyperfine features are observed on the parallel side of the spectra where as the fourth one has been overlapped on perpendicular features of the spectra. However, perpendicular hyperfines are not resolved leading to an intense band in the high field region (indicating that width of an individual line is exceeding the separation between them). The ESR spectra are analyzed using spin Hamiltonian.

$H = g_{//}\beta H_z S_z + g_{\perp}\beta (H_x S_x + H_y S_y) + A_{//} S_z I_z + A_{\perp} (S_x I_x + S_y I_y)$

where z is the symmetry axis of the individual copper centers, β the Bohr mageton, S and I are the electron and nuclear spin operators, H_x, H_y and H_z are the static magnetic field components, $g_{//}$ and $g_{\perp}$ are the parallel and perpendicular components of the g tensor and $A_{//}$ and $A_{\perp}$ are parallel and perpendicular components of the hyperfine tensor A and the nuclear quadrupole interaction has been neglected. The values of $A_{//}$ are calculated using the following equation [17].

$H_{//}(-3/2) - H_{//}(+3/2) = 3A_{//}$

The spin Hamilton parameters of glass series have been calculated and are presented in table 7.

Table 7 Spin Hamiltonian parameters of *xMgO-10Nb_2O_5-(89-x) TeO_2-1CuO glass system.*

Glass label	$g_{//}$(±0.002)	$g_{\perp}$(±0.002)	$A_{//}$ (10^{-4}cm^{-1})	$A_{\perp}$ (10^{-4}cm^{-1})
MNT1	2.356	2.076	122±2	63±2
MNT2	2.386	2.076	91±2	51±2
MNT3	2.358	2.076	122±2	63±2
MNT4	2.348	2.084	122±2	72±2
MNT5	2.353	2.076	122±2	63±2

From the spin Hamiltonian parameters, it is found that $g_{//} > g_{\perp}$ i.e. Cu^{2+} is in an octahedral coordination with tetrahedral distortion. The ground state of Cu^{2+} is $d_{x^2-y^2}$. The anisotropic hyperfine structure is due to Jhan-Teller distortion. As the content of MgO increases there are perceptible changes in $g_{//}$, $g_{\perp}$, $A_{//}$ and $A_{\perp}$ values. This indicates that structural changes are taking place in the present glass system with MgO content. These spin Hamiltonian parameters are in good agreement with the earlier reported values [18-23].

Optical absorption spectra

Divalent copper has a $3d^9$ electronic configuration; the $3d$ level splits to ^2E_g and $^2T_{2g}$ in a ligand-field of cubic symmetry. However, as the ground state for divalent Cu in an octahedral ligand field is ^2E_g, tetragonal splitting due to Jhan-Teller distortion will occur and must be considered when analyzing the spectrum. In a tetragonal field ^2E_g level splits to $^2B_{1g}$ and $^2A_{1g}$ and $^2T_{2g}$ level to $^2B_{2g}$ and ^2E_g .

The optical absorption spectra of glass series is shown in figures 7, There exists only one broad absorption band near 810 nm in all glass systems. The peak positions for the present glass samples are given table 8.

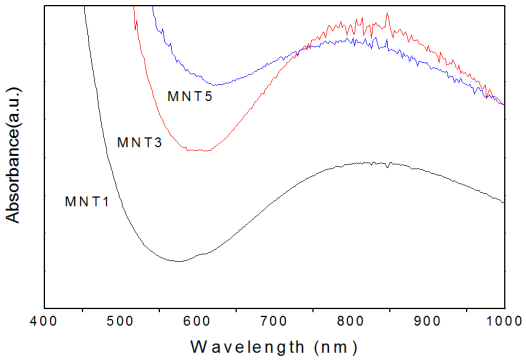

Fig. 7 The optical absorption spectra of Cu^{2+} in MNT1, MNT3 and MNT5 glasses.

Table 8 Absorption peaks of Cu^{2+}, bonding parameters and bonding symmetry of Cu^{2+} doped in *xMgO-10Nb_2O_5-(89-x)TeO_2-1CuO glass* system.

Glass label	Cu^{2+} peak (nm)	α^2	β^2	β_1^2	τ_π (%)	τ_σ (%)
MNT1	822	0.7673	1.0021	0.9119	17.60	50.71
MNT2	815	0.7112	1.0811	0.9226	15.47	62.92
MNT3	810	0.7693	0.9995	0.8584	28.32	50.27
MNT4	805	0.7628	1.1861	0.8486	30.27	51.69
MNT5	800	0.7643	1.0060	0.8648	27.03	51.36

The variation of peak position with MgO content indicates the fluctuations in ligand field around Cu^{2+} probe due to producing of non-bridging oxygen ions. The absorption band around 810 nm is due to presence of Cu^{2+} and can be assigned to $^2B_{1g} \rightarrow {}^2B_{2g}$ transition [24, 25].

The bonding parameters are calculated using ESR and optical absorption data using the following equations [17, 26].

$$g_{//} = 2.0023\ [\ 1\text{-}4\ \lambda\ \alpha^2\ \beta_1{}^2 /\ E_{xy}\ ]$$

$$g_{\perp} = 2.0023\ [\ 1\text{-}\ \lambda\ \alpha^2\ \beta^2 /\ E_{xz,\ yz}\ ]$$

where λ, spin orbit coupling parameter is equal to 828 cm^{-1} for Cu and $\beta^2 \cong 1$ for octahedral environment. E_{xy} and $E_{xz,\ yz}$ are the heights of the d_{xy} and $d_{xz,\ yz}$ and molecular orbital levels above the ground state, $d_{x^2-y^2}$, respectively and these values are estimated from optical absorption spectra [27]. In the optical absorption spectra, the position of observed absorption maximum of Cu^{2+} indicates the values of E_{xy}. The frequency position $E_{xz,\ yz}$ depend on the assumption that Cu^{2+} is in a distorted octahedral environment and is calculated by

$$E_{xz,\ yz} = 2k^2\lambda / 2.0023 - g_{\perp}$$

where k, the orbital reduction factor is equal to 0.77 and remaining terms have their usual meanings.

The in-plane σ-bonding parameter, α^2 is calculated using the following equation [24, 28].

$$\alpha^2 = \frac{7}{4}\left(\frac{A_{\parallel}}{P} \quad \frac{A}{P} \quad \frac{2}{3}g_{\parallel} \quad \frac{5}{21}g_{\perp} \quad \frac{6}{7}\right)$$

where P = 0.036 cm^{-1} and A = $(1/3A_{\parallel} + 2/3\ A_{\perp})$.

The normalized covalency of Cu^{2+}- O in-plane bonding of σ and π symmetry are calculated by using following equations:

$\Gamma_{\sigma} = 200(1\text{-}S)(1\text{-}\alpha^2) / (1\text{-}2S)$ (%) and

$\Gamma_{\pi} = 200(1\text{-}\beta_1{}^2)$ (%)

where S is the overlap ($S_{oxygen} = 0.076$).

As shown in table 8, the bonding parameters are changing with the mol% of MgO. The bonding coefficients α^2, $\beta_1{}^2$ and β^2 characterize respectively, the in-plane σ bonding, in-plane π bonding and out-of plane π bonding of the copper (II) complex. The α^2 values lie between 0.5 and 1.0, the limits of pure covalent and pure ionic bonding. From table 8, it is clear that, there is a covalancy for the in-plane σ-bonding and the in-plane π-bonding is ionic in nature. It is observed that normalized covalency of Cu^{2+}- O in-plane bonding of σ symmetry (Γ_{σ}) and normalized covalency of Cu^{2+}-O in-plane bonding of π symmetry (Γ_{π}) are changing with MgO content.

CONCLUSIONS

1. The density, oxygen packing density and glass transition temperature are increasing while molar volume and glass stability are decreasing with increase in the MgO content.
2. From Raman and IR spectroscopies, it is concluded that glass systems consisting of TeO_4 (tbp), TeO_3 (tp) and Nb_2O_5 octahedra and TeO_4 units are converting to TeO_3 units as MgO content increases.
3. From ESR and optical absorption data, it is found that the Cu^{2+} ions occupy tetragonally distorted octahedral sites elongated along z-axis with $d_{x^2-y^2}$ as the ground state.
4. The optical absorption spectra of the glasses show a single broad band due to $^2B_{1g} \rightarrow {}^2B_{2g}$ transition of Cu^{2+} ions in axially elongated octahedral sites. And the observed optical absorption peak of Cu^{2+} is found to be maximum at 810 nm.
5. The bonding parameters calculated from both optical and ESR data are found to change with MgO content. Thus it can be concluded that structural changes are taking place in the present system, with the change of MgO content.

Acknowledgments

The authors thank Dr. C. Manjulatha, Principal, Government City College (A), Hyderabad, for her encouragement and support. The authors are also grateful to Dr. A. M Awasthi and Dr. Vasant sathe for providing the MDSC and Raman measurements respectively. Authors also thank Director, CFRD, OU for FTIR measurements. One of the author (Dr. J Chinna Babu) is grateful to UGC (University Grants commission), New Delhi, for providing financial assistance under the scheme 'Minor Research Project' No. F. MRP4714/14 (SERO/UGC).

References

1. M. J. Waber, J. D. Meyers, D. H. Blackburn, *J. Appl. Phys*., 52 (1981) 2944.
2. M.A.P. Silva, Y. Messaddeq, S.J.L. Ribeiro, M, Poulain, F.Villain, V. Briois, *J. Phys.Chem. Solids* 62 (2001) 1055
3. G .Vijay prakash, D. Narayana Rao, A. K. Bhatnagar, Solid State Commun., 119 (2001) 39.
4. T. Kokubo, Y .Inaka, S. Sakka, *J. Non-Cryst. Solids*, 81 (1986) 337.
5. Arspreet Kaur, Atul Khanna, Vasant G. Sathe, Fernando Gonzalez, Belen Ortiz, Phase Transitions 86 (6) (2013) 598.
6. K. Tanaka, T. Yoko, H. Yamada, K. Kamiya, *J. Non-Cryst. Solids*, 103 (1988) 250.
7. C. Duverger, M. Bouazaoui, S. Turrell, *J. Non-Cryst. Solids* 220 (1997) 169.
8. T.Komatsu, N. Ito, T.Honma, V.Dimitrov Solid State sciences 14 (2012) 1419.
9. K. Fukumi, S. Sakka, *J. Non-Cryst. Solids*, 110 (1989) 61.
10. T. Komatsu, H. Tawarayama, H. Mohri, K. Matusita, *J. Non-Cryst. Solids*, 135 (1991) 105.
11. Fabia C. Cassanjes, Younes Messaddeq, Luiz F. C. de Oliveira, Lilia C. Courrol, Laercio Gomes Sidney, *J. L. Ribeiro*, *J. Non-Cryst. Solids*, 247 (1999) 58.
12. S. Surendra babu, K. Jang, E. J. Cho, V. Lee, C. K. Jayasankar, Phys.D: Appl. Phys., 40 (2007) 5767.
13. F. F. Sene, J. R, Martinelli, L. Gomes, *J. Non-Cryst.Solids*, 348 (2004) 30.
14. P. Charton, P. Armand, *J.Non-Cryst.Solids*, 316 (2003) 189.
15. P. Charton, P. Armand, J.Non-Cryst.Solids, 333 (2004) 307.
16. E. B. DE Araujo, J. A. C. DE Paiva, J. A. Freitas JR., A. S. B. Sombra, *J. Phys.Chem. Solids*, 59 (1997) 689.

17. D. Kivolson D, S. K. Lee, J. Chem. Phys., 47 (1986) 11.
18. J. Chinna Babu, S. Suresh,V. Chandra Mouli, Indian J. Pure & Appl. Phy., 43 (2005) 833.
19. N .Chopra, A .Mansingh, P. Mathur, *J. Non-Cryst. Solids*, 146 (1992) 261.
20. S. Suresh S, J. Chinna Babu, V. Chandra mouli, Phys. Chem. Glasses, 46 (2005) 27.
21. A. Yadav, V.P. Seth, S. K. Gupta, *J. Non-Cryst. Solids*. 101 (1988) 1.
22. Swapna, G.Upender, M.Prasad, Optik 127 (2016)
23. G.Upender, J.Chinna Babu, V.Chandra Mouli, Spectrochimica Acta Part A 89 (2012) 39.
24. R.P.S. Chakradhar, B. Yasoda, J. L. Rao, Gopal, J.Non-Cryst.Solids, 352 (2006) 3864.
25. S. Sakka, K. Kamira, K. Makita, Yamanoto, J.Non-Cryst.Solids, 63 **(**1984) 223.
26. S. Hazra, A. Ghosh, Phys. Rev. B, 51 (1995) 851.
27. J. Krogh-Moe, *Phys*. Chem. Glasses, 6 (1965) 46.
28. H. A. Kuska, M. T. Rogers, R. E. Durllinger, J. Phys. Chem., 71 (1967) 109.

****